

On the Mandelbrot Set for $i^2 = \pm 1$ and Imaginary Higgs Fields

Jonathan Blackledge

Stokes Professor, Science Foundation Ireland.
Distinguished Professor, Centre for Advanced Studies,
Warsaw University of Technology, Poland.
Visiting Professor, Faculty of Arts, Science and Technology,
Wrexham Glyndwr University of Wales, UK.
Professor Extraordinaire, Faculty of Natural Sciences,
University of Western Cape, South Africa.
Honorary Professor, School of Electrical and Electronic Engineering,
Technological University Dublin, Ireland.
Honorary Professor, School of Mathematics, Statistics and Computer Science,
University of KwaZulu-Natal, South Africa.
Email: jonathan.blackledge@TUDublin.ie

Abstract We consider the consequence of breaking with a fundamental result in complex analysis by letting $i^2 = \pm 1$ where $i = \sqrt{-1}$ is the basic unit of all imaginary numbers. An analysis of the Mandelbrot set for this case shows that a demarcation between a Fractal and a Euclidean object is possible based on $i^2 = -1$ and $i^2 = +1$, respectively. Further, we consider the transient behaviour associated with the two cases to produce a range of non-standard sets in which a Fractal geometric structure is transformed into a Euclidean object. In the case of the Mandelbrot set, the Euclidean object is a square whose properties are investigate. Coupled with the associated Julia sets and other complex plane mappings, this approach provides the potential to generate a wide range of new semi-fractal structures which are visually interesting and may be of artistic merit. In this context, we present a mathematical paradox which explores the idea that $i^2 = \pm 1$. This is based on coupling a well known result of the Riemann zeta function (i.e. $\zeta(0) = -1/2$) with the Grandi's series, both being examples of Ramanujan sums. We then explore the significance of this result in regard to an interpretation of the fundamental field equations of Quantum Mechanics when a Higgs field is taken to be produced by an imaginary mass im such that $(\pm im)^2 = +m^2$. A set of new field equations are derived and studied. This includes an evaluation of the propagators (the free space Green's functions) which exhibit decay characteristics over very short (sub-atomic) distances.

Keywords: non-standard Mandelbrot set, transient characteristics, imaginary mass, causal tachyons, Higgs fields.

1 Introduction

In complex analysis [1], $i = \sqrt{-1}$ is the basic unit of all imaginary numbers. It is taken by default that $i^2 = -1$ which appears to be the only rational way in which the unit of an imaginary number can conform to a real number system consisting of numbers in both the negative and positive half space. In this paper, we study the effect of breaking with this fundamental result and consider the case when $i^2 = \pm 1$. We show that this has a significant effect on the result of iterating non-linear maps in the complex plane. For the Mandelbrot set [2], it is revealed that we can distinguish between a self-similar Fractal structure [3] and a Euclidean [4] structure (namely, a square) on the basis of whether $i^2 = -1$ or $i^2 = +1$, respectively. Consequently, we study the transitory behaviour of a Mandelbrot set to investigate the structures that are obtained as i^2 changes from -1 to $+1$.

The prototype .m code used to undertake this study is presented in an appendix which consists of two MATLAB functions for computing the non-standard Mandelbrot and non-standard Julia sets (e.g. [5] and [6]) together with other non-analytic sets. The code is provided to give interested readers an opportunity to repeat the results presented in this paper and to explore new results above and beyond those that are considered in this work. The principal purpose of this approach is to investigate the structural complexity of the Mandelbrot and Julia sets (and other non-analytic maps) when we break with one of the most basic

rules of complex analysis. This leads to a range of new and original images that are visually interesting and may be of value in an artistic sense. In this context, breaking with the standard result that $i^2 = -1$ is inconsequential. However, at a deeper level, such a break with convention offers a route to some more fundamental analysis in mathematics and theoretical physics which is also investigated in this work. In this respect, we introduce an analysis that yields a mathematical paradox using the Riemann Zeta Function [7] and the Grandi's series [8]. Based on a Ramanujan summation for assigning values to a divergent series, the analysis presented appears to justify a case for $i^2 = \pm 1$. On the basis of this result, we explore the effect of breaking with convention in regard to the study of an imaginary mass and the characteristics of the Tachyonic fields generated by particles with an imaginary mass [9].

For a particle with an imaginary mass im , it is shown that if $(\pm im)^2 = +m^2$, such a particle can conform to the principle of causality in the sense that no particles can travel faster than light speed. This has consequences for the Partial Differential Equations that define the fields for both a relativistic and non-relativistic quantum mechanical system. Using a one-dimensional analysis, we study the Klein-Gordon equation [10] whose wave function describes scalar Bosons [11] and show that if $(\pm im)^2 = +m^2$, the equation must include an additional term which depends on the gradient of the Higgs field [12], a field that accounts for the physical manifestation of mass through the Higgs Boson as verified experimentally in 2015 [13]. The propagator (i.e. the free space Green's function) for this new case is derived and its basic characteristics (in regard to its spatial decay) briefly studied and quantified.

2 Structure of the Paper

Section 3 revisits the principles of iteration in the complex plane, considers the basis for computing the Mandelbrot set and Julia sets and briefly reviews some of their properties which is presented in Section 4. The purpose of this is to inform readers who are not familiar with the iteration of non-linear functions in the complex plane and the analysis thereof. Section 5 then introduces some examples of generating non-analytic sets such as the 'Mandelbar set' and the further generalisations of non-linear iterations. This provides a short background to an original contribution which is the study on the non-standard Mandelbrot set. This is the Mandelbrot set that is obtained when $i^2 = +1$ as presented in Section 6. This section also includes some examples of non-standard Julia sets and the transient characteristics of such iterations when i^2 is taken to change between -1 and $+1$ leading to objects that have both self-affine and Euclidean characteristics - 'Semi-fractals'.

Section 7 explores a paradox associated with the question as to whether $i^2 = \pm 1$ in order to provide an analysis to complement the basis (a fundamental break with convention) upon which the results given in Section 6 are conceived. This leads to a study of Tachyonic fields as given in Section 8 which discusses the issue of causality in the context of an imaginary mass. Section 9 then provides a brief review on the fundamental equations of Quantum Mechanics, specifically, the derivation of the Dirac equation for a one-dimensional case. This provides a background for the analysis presented in Section 10 which formulates new quantum field equations based on a complex plane analysis when $i^2 = +1$. The propagator characteristics of these fields are explored in Section 11 through an evaluation of the corresponding free space Green's functions. Sections 12 and 13 provide a conclusion to the work and some ideas for further analysis, respectively.

3 Iteration in the Complex Plane Revisited: The Mandelbrot and Julia Sets

Consider a complex function $f(z)$ where $z = x + iy$ is the complex independent variable. Iteration in the complex plane then involves an analysis of the iterative equation

$$z_{n+1} = f(z_n), \quad n = 1, 2, 3, \dots \quad (1)$$

for some initial condition z_0 . This iteration represents the application a map which is denoted by

$$f : z \rightarrow f(z), \quad z \in \mathbb{C}$$

Referred to as the trajectory or 'orbit' (in the complex plane), the sequence of complex values z_n that is produced by this iteration will depend on the function $f(z)$ and the initial condition z_0 that is applied.

When $f(z)$ is a linear function, the iteration may or may not converge depending upon the characteristic of the function and its parameters (coefficients and constants, for example). However, when the function is non-linear, the iteration may give rise to a range of different orbits in the complex plane which are characterised by divergence, convergence, periodicity or chaos.

A divergent orbit is one where the value of z_n continually increases in value as the iteration progresses and is said to ‘escape to infinity’ as $\Re[z_n]$ and/or $\Im[z_n] \rightarrow \infty$ as $n \rightarrow \infty$ where \Re and \Im denote the real and imaginary components of the complex value z_n at any iteration n , respectively. A convergent orbit is one that tends to a specific point in the complex plane (a constant complex number). A periodic orbit is one that oscillates between two numbers with a given periodicity which may involve different fixed or variable cycles. If the orbit is chaotic, then the values of z_n are taken to have no specific pattern as the iteration progresses. In this context, the analysis of Equation (1) can be divided into observing two specific characteristics; the points in the complex plane when the orbit diverges or ‘escapes to infinity’ and those points in the complex plane when the orbit does not escape to infinity and is either convergent, cyclic or chaotic. By analysing the patterns in the complex plane that emerge through the implementation of this distinction, self-similar and/or self-affine structures become apparent whose features and complexity are determined by the specific function $f(z)$ and the initial conditions that are considered. The self-affine characteristics of the complex map that is obtained are typically revealed in terms of the boundary that represents the demarcation between the two cases. This is the basic principle upon which fractal structures can be generated from Equation (1).

The Mandelbrot set and the Julia sets [14], [15] are concerned with a study of the orbits when $f(z)$ is a quadratic, i.e. $f : z \rightarrow z^2 + c$ and variations upon this theme. Thus, the basic iteration that we are interested in studying is given by

$$z_{n+1} = z_n^2 + c, \quad n = 1, 2, 3, \dots$$

where c is a complex constant for some initial condition z_0 . There are two approaches that can be considered in this respect. We can analyse the iteration for a fixed value of c and different initial condition z_0 or we can analyse the iteration for different values of c for the same initial condition z_0 . The difference between these two approaches defines the difference between the Julia set and the Mandelbrot set, respectively, where, in the latter case the initial condition is $z_0 = 0 + i0$. Hence, we can formally define the Mandelbrot set and Julia sets as follows:

- (i) The Mandelbrot set is the set of complex numbers c for which the complex function $f(z) = z^2 + c$ does not diverge when iterated for the initial condition $z_0 = 0 + i0$.
- (ii) A Julia set is the set of complex numbers z for which the complex function $f(z) = z^2 + c$ does not diverge when iterated for a fixed value of c and different initial condition z_0 .

If we restrict the analysis of the set of complex numbers to a specific rectilinear region of the complex plane so that $x \in [-X, X]$ and $iy \in [-Yi, Yi]$, then it is clear that there can be many Julia sets obtained for different values of c , but that there is only one Mandelbrot set, at least for the case when $z_0 = 0$. Further, if we define a subset of the complex plane to be

$$K(f) = \{z \in \mathbb{C} : \forall n \in \mathbb{N}, |f^n(z)| \leq R\}$$

where $f^n(z)$ is the n^{th} iterate of $f(z)$ and R is some upper bound, then a Julia set $J(f)$ of this function is the boundary of $K(f)$. For the Mandelbrot set $|c| \leq 2$ and for this reason (of compatibility) we set $R = 2$.

In both cases, the output is viewed in the complex plane that c or z defines (for the Mandelbrot and Julia set, respectively). Thus, both sets consists of all of those values in the complex plane for which the corresponding orbits under the map $z \rightarrow z^2 + c$ do not ‘escape to infinity’. Figure 1 shows the Mandelbrot set (left) and an example Julia set (right) when $c = -0.835 + 0.2321i$, for $x \in [-2, 2]$, $iy \in [-2i, 2i]$ computed over a $10^3 \times 10^3$ grid for 100 iterations. These results have been generated using MATLAB based on the .m code which is given in the Appendix and will be discussed later on. The data is displayed using a continuously coloured environment. For this purpose the MATLAB colour map ‘jet’ (which is a ‘heat map’) has been used to display the sets given in Figure 1.

In both cases, the central complex structured components of the images shown in Figure 1 are displays of those regions in the complex plane where the orbits do not tend to infinity. The decentralised components of these maps (with the uniform background dark-red colour) are those regions in the complex plane where the orbits do ‘escape’ tending to infinity as the iterations proceed. In the practice of computing and graphing sets of this type, the numerical floating point values that are obtained after a finite number of iterations are normalised, quantised and presented as a 24-bit pseudo-colour map (as given in Figure 1). Other colour maps can be applied including grey-level displays of the data.

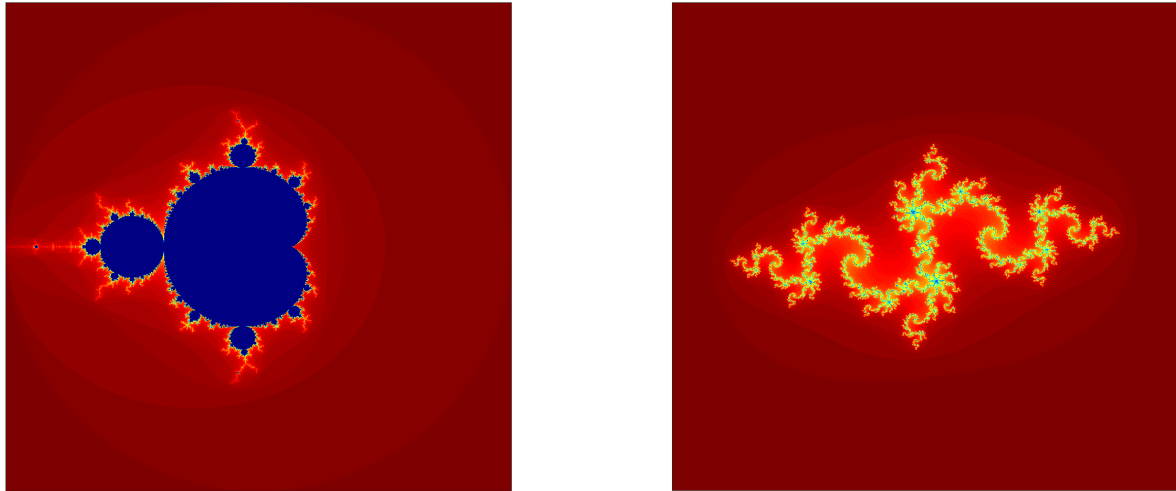


Figure 1. The Mandelbrot set (left) and a Julia set for $c = -0.835 + 0.2321i$ (right). Both sets are computed for $x \in [-2, 2]$ (horizontal axis) and $iy \in [-2i, 2i]$ (vertical axis) using a $10^3 \times 10^3$ grid and 100 iterations. Both maps have been presented using the MATLAB ‘jet’ colour map.

4 Some Basic Properties

4.1 The Mandelbrot Set

The Mandelbrot set shown in Figure 1 consists of the central region - the ‘main cardioid’ - with a secondary attached ‘bulb’ to the left. This basic structure is repeated periodically along the boundary at smaller and smaller scales. The set is therefore an example of a self-similar object, a fractal with a boundary Hausdorff dimension of 2. The dark-blue areas of the set are those regions in the complex plane where the orbits do not diverge and ‘escape to infinity’ as $n \rightarrow \infty$. The set is symmetric in the imaginary plane, i.e. the set for $iy \in [-2i, 0i]$ is a mirror image of the set for $iy \in [0i, 2i]$. For the real axis, the set exists over the interval $x \in [-2, 1/4]$ where the point $x = 0$ lies within the main cardioid and the point $x = -1$ lies within the left bulb.

The Mandelbrot set is an example of a compact set. This is because it is closed and contained in a closed disk of radius 2 around the origin. More specifically, a point c belongs to the Mandelbrot set if and only if $|z_n| \leq 2 \forall n \geq 0$, i.e. the absolute value of z_n must remain at or below 2 for c to be in the Mandelbrot set; if the absolute value exceeds 2, the sequence will escape to infinity.

4.2 Julia Sets

Julia sets are specific for a chosen and fixed value of c associated with the map $z \rightarrow z^2 + c$. Each map (a filled Julia set) is different to the next and vary significantly in their construction and complexity with some specific commonality. This is illustrated in Figure 2 which shows two example Julia sets for

$c = -0.4 - 0.6i$ and $c = 0.285 + 0.01i$. Filled Julia sets fall into two principal categories. They are either connected sets (i.e. consist of one component alone) or consist of infinitely many components, each of which is a single point. In the latter case, the Julia set produces a point cloud or Cantor set.

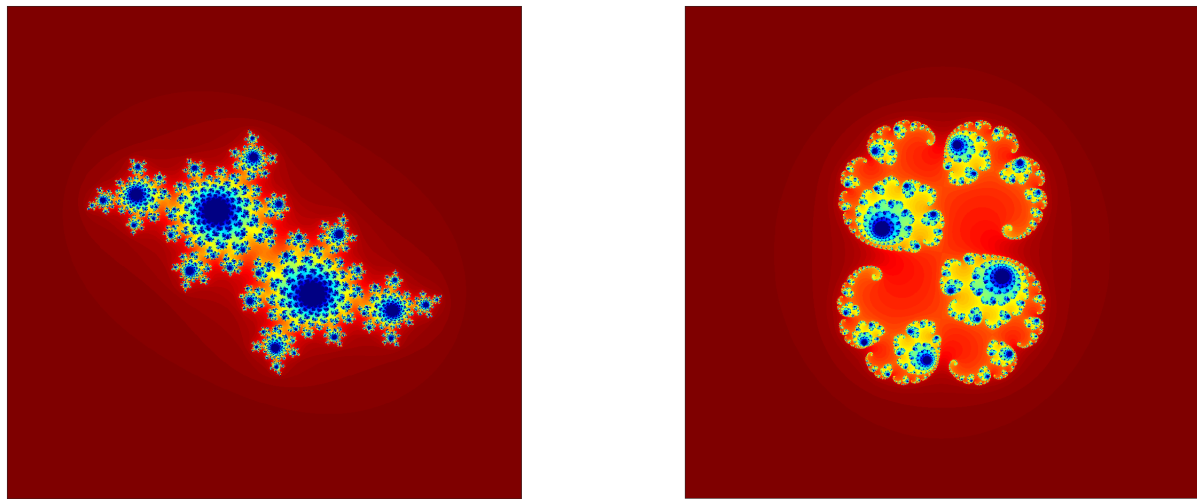


Figure 2. The Julia set for $c = -0.4 - 0.6i$ (left) and the Julia set for $c = 0.285 + 0.01i$ (right) computed over $x \in [-2, 2]$ (horizontal axis) and $iy \in [-2i, 2i]$ (vertical axis) using a $10^3 \times 10^3$ grid for 100 iterations and displayed using the MATLAB ‘jet’ colour map.

5 Non-analytic Mappings and Generalisations

There are many ‘variations on the theme’ associated with computing Mandelbrot and Julia sets that can be investigated. Some examples of such maps are briefly discussed in this section in order to introduce to the reader the idea that one is free to invent a wide range of complex plane iterations that do not necessarily have to conform to convention and study their outputs. These are examples of non-analytic mappings because they do not conform to the Cauchy-Riemann equations.

5.1 The Mandelbar Set

The Mandelbrot set is compounded in the mapping [14]

$$f : z \rightarrow \bar{z}^2 + c, \quad z \in \mathbb{C} \quad (2)$$

where \bar{z} denotes the conjugate of the complex variable z . This is a non-analytic mapping, and, in comparison with the results shown in Figure 1, produces the results given in Figure 3. Here, the Mandelbrot set transforms to a Tricorn often referred to as a Mandelbar set because of the notation used to denote a complex conjugate where $\bar{z} \equiv z^*$. Unlike the Mandelbrot set, the Mandelbar set associated with Equation (2) has a centre of gravity at $z = 0 + 0i$. It consists of three self-affine projections, each of which are symmetric about the line of projection with complex plane angles or ‘phases’ of $\pi/3$, π and $5\pi/3$. The central component of this set is not self-affine as it has well defined convex curves each with a definable edge. It is therefore an example of a connected set that has both Euclidean and Fractal properties over different regions of the complex plane - a ‘Semi-fractal’. The effect on the non-analytic Julia set associated with Equation (2) is to dissipate the locality of the set shown in Figure 1. The set is isometric in the sense that a reflection in the real and complex planes reproduces the set.

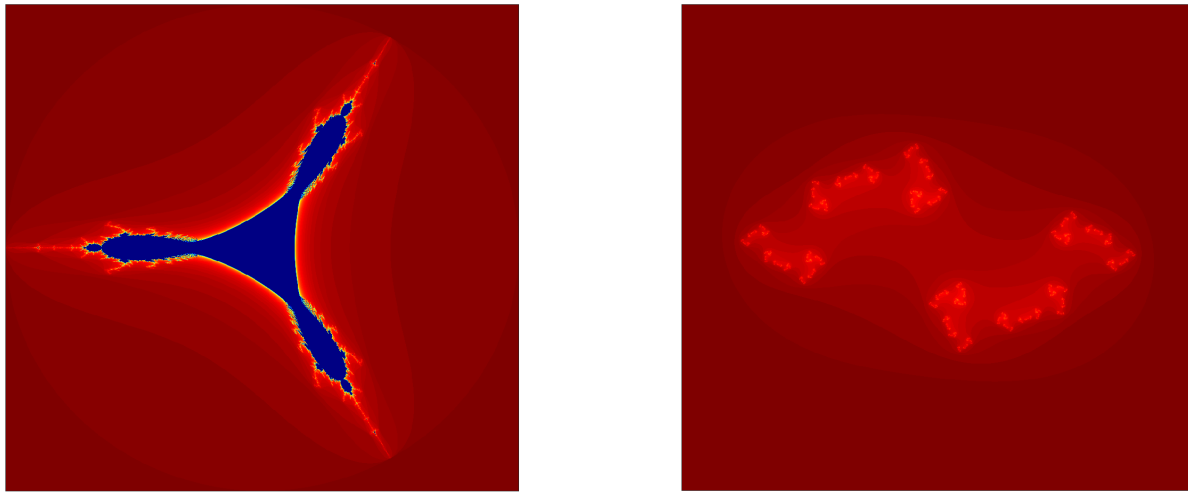


Figure 3. The ‘Mandelbar’ set (left) and an associated Julia set for $c = -0.835 + 0.2321i$ (right) obtained using the mapping $z \rightarrow \bar{z}^2 + c$, both sets being computed for $x \in [-2, 2]$ (horizontal axis) and $iy \in [-2i, 2i]$ (vertical axis) using a $10^3 \times 10^3$ grid, 100 iterations and the MATLAB ‘jet’ colour map.

5.2 Multibrot Sets

A Multibrot set is one that is based a generalisation of the Mandelbrot set to include an arbitrary power exponent d leading to a family of iterations based on the map

$$f : z \rightarrow z^d + c, z \in \mathbb{C} \quad (3)$$

where $d \in (-\infty, \infty)$, i.e. where z can have positive, negative or fractional powers. The same approach can be taken to produce a family of multi-Julia sets. Thus, the Mandelbrot set becomes the case for $d = 2$. For positive integer values of $d > 2$ the sets consist of $d - 2$ cardioids, each with a secondary attached bulb, the centre of gravity of all such sets being at $0 + 0i$.

5.3 The Burning Ship Fractal

The ‘Burning Ship Fractal’ (BSF) is based on the iteration [16]

$$z_{n+1} = (|\Re[z_n]| + i |\Im[z_n]|)^2 + c, z_0 = 0 \quad (4)$$

and is shown in Figure 4 together with a non-analytic Julia set for $c = 0.25 + 0.15i$. The BSF is highly asymmetric where as the Julia for this value of c is symmetric in the complex plane.

6 Non-standard Mandelbrot and Julia Sets

In the definition, analysis and visualisation of all the complex plane sets considered in the previous sections, a fundamental result has been assumed, namely that $i^2 = -1$. Given that $i = \sqrt{-1}$ is the basic unit of all imaginary numbers, the equation $i^2 = -1$ is fundamental to relating any imaginary number system conform to a real number system with both positive and negative values. Nevertheless, i is still imaginary; meaning that it can not be defined and is, in effect a fictitious number. In this context, let us now consider a fictitious and non-standard result that is inconsistent with (conventional) complex analysis and where $i^2 = +1$ (non-standard) as well as $i^2 = -1$ (standard). Here, i is still taken to be equal to $\sqrt{-1}$ but has the property that $i^2 = \pm 1$. What are the ramifications for the in terms of the geometry of a Mandelbrot set, a Julia set and beyond?

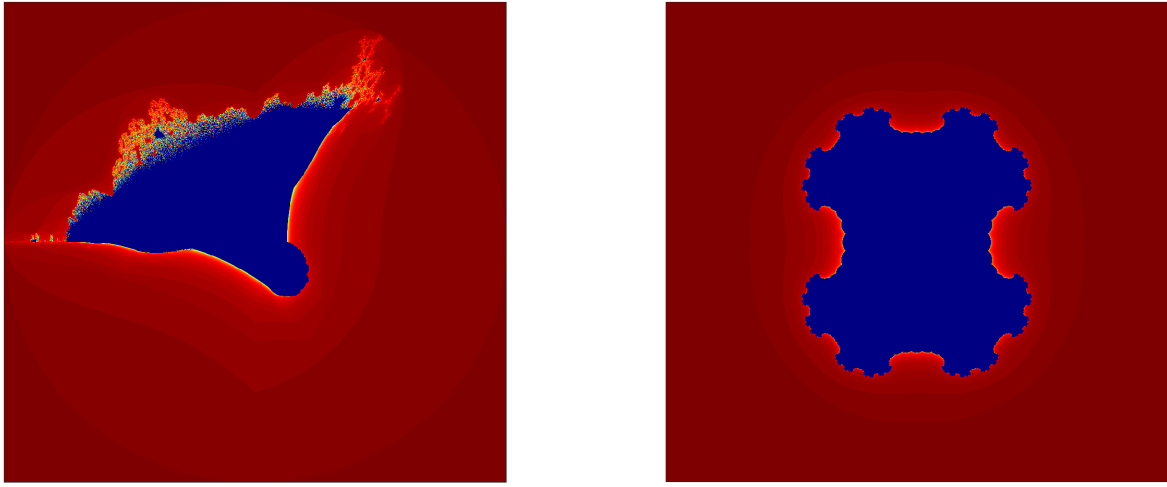


Figure 4. The ‘Burning Ship Fractal’ (left) and a (non-analytic) Julia set for $c = 0.25 + 0.15i$ (right) obtained using the iteration given by Equation (4), both sets being computed for $x \in [-2, 2]$ (horizontal axis) and $iy \in [2i, -2i]$ (vertical axis) using a $10^3 \times 10^3$ grid and 100 iterations. The colour map used to display these results is the MATLAB ‘jet’ colour map.

6.1 Non-standard Mandelbrot Set

If $z = x + iy$, then the map $f : z \rightarrow z^2 + c$, $z \in \mathbb{C}$ has an iteration that can be written as

$$z_{n+1} = z_n^2 + c$$

or, in terms of real and imaginary parts

$$z_{n+1} = z_n^2 + c = \Re[z_n]^2 - \Im[z_n]^2 + 2i\Re[z_n]\Im[z_n] + c \quad (5)$$

given that $i^2 = -1$. However, suppose we consider the case when $i^2 = +1$. In this case, the iteration becomes

$$z_{n+1} = z_n^2 + c = \Re[z_n]^2 + \Im[z_n]^2 + 2i\Re[z_n]\Im[z_n] + c \quad (6)$$

which is of course equivalent to the iteration

$$z_{n+1} = |z_n|^2 + 2i\Re[z_n]\Im[z_n] + c$$

Figure 5 shows the difference between the iteration schemes for Equation (5) and Equation (6) where $z_0 = 0 + 0i$ for $x \in [-2, 1]$ and $iy \in [-1.5i, 1.5i]$, a $10^3 \times 10^3$ grid and 100 iterations.

In studying the maps shown in Figure 5, it is apparent that there is a dramatic change from a Fractal (a self-similar object) to a ‘Euclid’ (a non-self-similar object) in the complex plane where we define a Euclid as a geometric object corresponding to a Euclidean geometry associated with ordinary experience. In the case of Figure 5, the Euclid is a square, and, unlike the Mandelbrot set, is symmetric with respect to both the imaginary axis and the real axis (shifted to the left of $x = 0$). On the real axis, the sets exist over the interval $x \in [-2, 1/4]$. Thus, the length of the hypotenuse of the equilateral triangles above and below the real axis is 2.25. From Pythagoras’ theorem, the length ℓ of any one of the four sides of the square is given

$$\ell = \sqrt{\frac{2.25}{2}} = \frac{\sqrt{2 + 0.25}}{\sqrt{2}} = \sqrt{2} \frac{\sqrt{1 + 0.25/2}}{\sqrt{2}} = \sqrt{1 + 0.125} = 1.060660171779821\dots$$

which is an irrational number, as is the combined length of the four edges which is given by $4.242640687119284\dots$. However, the area of the square is given by $\ell^2 = 1.125 = 1125/1000$ and is therefore a rational number.

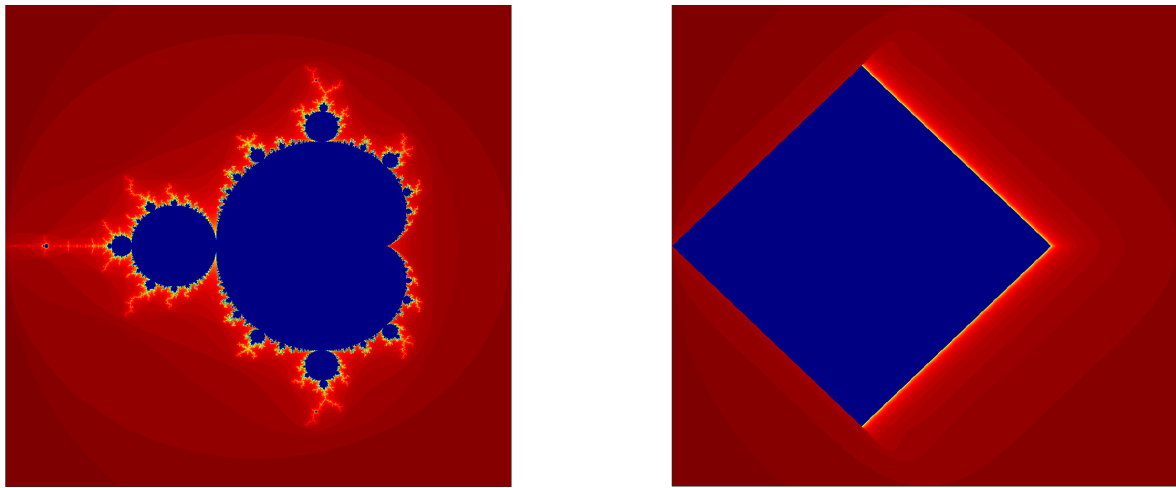


Figure 5. The conventional Mandelbrot set (left) based on Equation (5) and the non-standard set (right) based on Equation (6). Both sets are computed for $x \in [-2, 1]$ (horizontal axis) and $iy \in [-1.5i, 1.5i]$ (vertical axis) for a $10^3 \times 10^3$ grid and 100 iterations. Both sets are displayed using the MATLAB ‘jet’ colour map.

In the context of Figure 5, it is compelling to differentiate between the specific Fractal (the Mandelbrot set) and a specific Euclid (the square) in the complex planes with regard to the following equations:

$$\text{Fractal} : f : z \rightarrow z^2 + c, i^2 = -1, z \in \mathbb{C} \quad (7)$$

$$\text{Euclid} : f : z \rightarrow z^2 + c, i^2 = +1, z \in \mathbb{C} \quad (8)$$

If we consider the Euclid given in Figure 5 to have a Topological Dimension $D_T = 2$, then the Fractal object (the Mandelbrot set) has a Fractal Dimension $D_F \in (1, 2)$. In both cases, the geometries of the each object are a manifestation of an infinite set of points with non-infinite values in the complex plane. In this respect, Figure 5 illustrates that we may at least define a square for the mapping given by Equation (8)

The fractal dimension (specifically, the Hausdorff dimension) for the boundary of the Mandelbrot set defined by the mapping of Equation (7) is 2 where the boundary and the set itself have the same Hausdorff dimension. Thus, the Hausdorff dimensions are the same for both the sets displayed in Figure 5 and defined by Equations (7) and (8). However, for the Euclid, a line (of finite extent) can be defined in terms of the gradient across a boundary. This is the (complex plane) boundary between those points in which the set converge and those points where it diverges, i.e. the edges of the square that yield a set of points defined by a delta function when $n \rightarrow \infty$.

An equivalent definition for a gradient can not be defined for a conventional Mandelbrot set because of its self-affine characteristics at all scales. In the context of a Mandelbrot set for $i^2 = \pm 1$, this provides a demarcation between a geometry that supports or otherwise differentiability; a demarcation between regularity and complexity. This is further illustrated in Figure 6 which shows the difference between the iteration schemes for Equation (5) and Equation (6) but with $i := -i$ for $z_0 = 0 + 0i$, $x \in [-2, 1]$ and $iy \in [-1.5i, 1.5i]$, for a grid size of $10^3 \times 10^3$ and 100 iterations.

6.2 Non-standard Julia Sets

Figure 7 shows the Julia sets that are equivalent to those given in Figure 2 but for the case when $i^2 = +1$. As is the case for the Mandelbrot set, the results yield objects that are not self-affine. In the first case (for $c = -0.4 - 0.6i$), the result is clearly a rectangle oriented at an angle of $3\pi/4$ radians in the complex plane with a centre of gravity at $0 + 0i$. For $c = 0.285 + 0.01i$, the result is a rectilinear ‘potential’ centred at $0 + 0i$ with an orientation of $\pi/2$ radians.

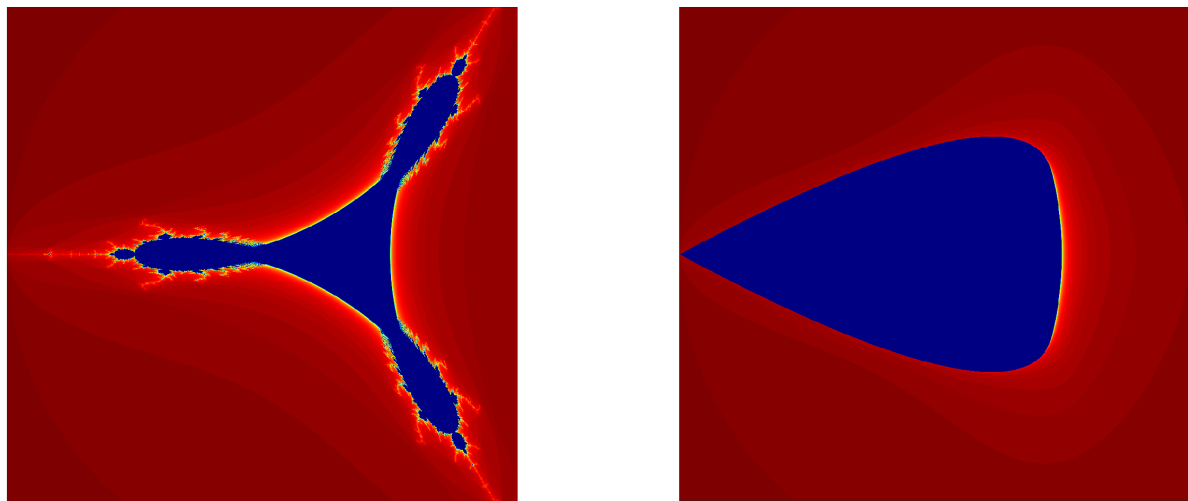


Figure 6. The set (left) based on Equation (5) with i changed to $-i$ and the set (right) based on Equation (6) with i also changed to $-i$. Both sets are computed for $x \in [-2, 1]$ (horizontal axis) and $iy \in [-1.5i, 1.5i]$ (vertical axis) for 100 iterations over a $10^3 \times 10^3$ grid displayed using a MATLAB ‘jet’ colour map.

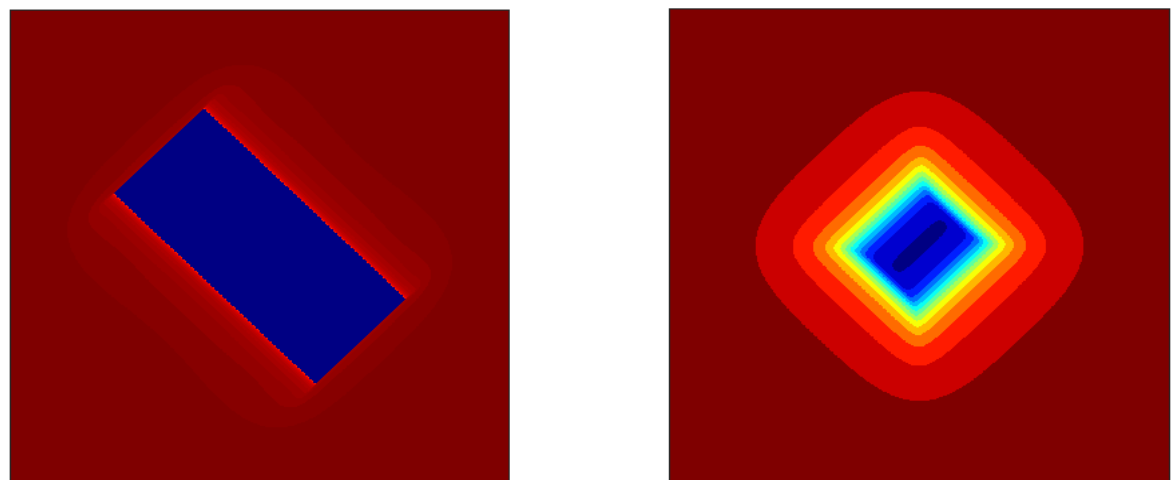


Figure 7. Non-standard Julia sets for $c = -0.4 - 0.6i$ (left) and the Julia set for $c = 0.285 + 0.01i$ (right) computed over $x \in [-2, 2]$ (vertical axis) and $iy \in [-2i, 2i]$ (horizontal axis) using a $10^3 \times 10^3$ grid and 100 iterations.

6.3 Transient Characteristics

Suppose we want to investigate the transition from the standard to non-standard Mandelbrot sets as $i^2 = -1$ transforms to $i^2 = +1$. One way to do this is to consider the iteration

$$x_{n+1} + iy_{n+1} = x_n^2 + \exp(i\alpha\pi)y_n^2 + 2ix_ny_n + c, \quad x_0 = 0, \quad y_0 = 0 \quad (9)$$

The Mandelbrot set is then recovered for all $\alpha = \pm 1, \pm 3, \pm 5, \dots$ (i.e. all positive and negative odd integers) and the non-standard map is obtained for all $\alpha = \pm 0, \pm 2, \pm 4, \dots$ (i.e. all positive and negative even integers including zero). Any values of α between an odd and even integer then provides the transitional behaviour from one map to the other.

Figure 8 shows an example of this transition for the Mandelbrot set based on Equation (9) for $\alpha = 1, 1.2, 1.4, 1.6, 1.8, 2$, with $x \in [-2, 1]$ and $iy \in [-1.5i, 1.5i]$.

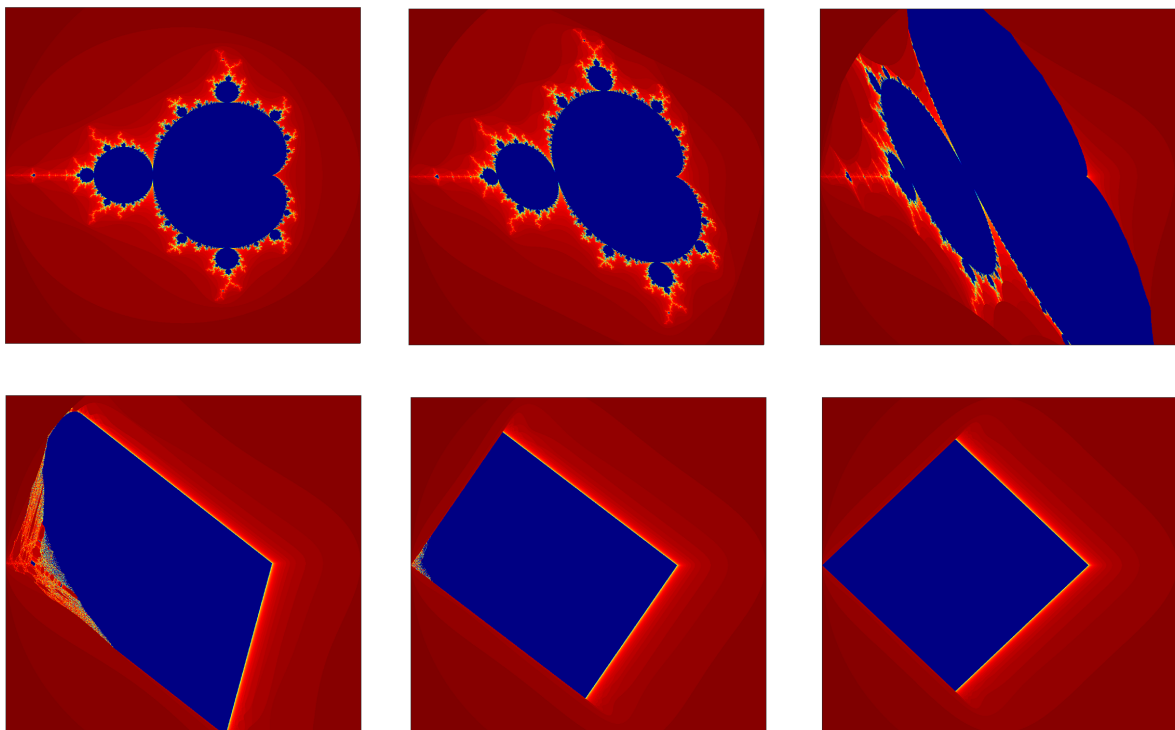


Figure 8. Transitions of the Mandelbrot set based on Equation (9) for $\alpha = 1, 1.2, 1.4, 1.6, 1.8, 2$ (top-left through to lower-right, respectively). The set is computed for $x \in [-2, 1]$ and $iy \in [-1.5i, 1.5i]$ where x and iy are the horizontal axis and vertical axis in the complex plane, respectively. In each case the set is compute using a grid size of $10^3 \times 10^3$ and 100 iterations. Each set is colour coded using the MATLAB ‘jet’ colour map.

6.4 Software Provision

In addition to the graphical results presented in this paper, provision is made for interested readers to repeat and verify these results and to further investigate the standard, non-standard and transient characteristics of the Mandelbrot set as discussed in Section 6.3, Julia sets and other sets based on the invention of non-analytic maps. For this purpose, two MATLAB [17] functions are provided in Appendix A and Appendix B whose use and operations are explained.

6.5 Discussion

While the application of $i^2 = +1$ to investigate Mandelbrot and Julia sets (and other mappings in the complex plane) can be implemented out of interest, it nevertheless raises an underlying issue. This is on how the result $i^2 = +1$ can be justified and interpreted. The rest of this paper is based on an investigation into this question and its potential ramifications. In the following section, we introduce an argument which appears to imply that $i^2 = +1$ is plausible. This is by way of a mathematical paradox, namely, a set of connected statements that lead to a contradiction while simultaneously seeming rational and logical. The paper then goes on to explore the application of $i^2 = +1$ in quantum physics, and, in particular, the role that it can play in re-defining the nature of a Higgs field generated by an imaginary mass.

7 Can $i^2 = \pm 1$? A Paradox based on the Riemann Zeta Function

For a complex variable s , the Riemann zeta function is given by [7]

$$\zeta(s) = \sum_{n=1}^{\infty} \frac{1}{n^s} \quad (10)$$

This series maps a value of s in the complex plane to a value of ζ in the complex plane and converges $\forall \Re[s] > 1$. However, the function has more general representations the lie beyond this condition. This is because the function is meromorphic throughout the whole complex plane and it is holomorphic everywhere except for a simple pole that occurs at $s = 1$ when it has a residue of 1.

Apart from $\zeta(1)$, when the function is undefined, this function has a range of different values for specific values of s . This includes the following:

$$\zeta(0) = \sum_{n=1}^{\infty} 1^n \equiv \sum_{n=1}^{\infty} 1 = 1 + 1 + 1 + \dots = -\frac{1}{2}$$

Given that $i^2 = -1$, this value of the zeta function immediately suggests the non-standard result

$$\sum_{n=1}^{\infty} i^2 = \frac{1}{2} \quad (11)$$

In the context of this result, we now consider a construction of the Grandi's series [8] as follows.

Let $i^2 = -1$, $j^2 = +1$,

$$x = \sum_{n=1}^{\infty} i^2 \text{ and } y = \sum_{n=1}^{\infty} j^2$$

Then the sum of x and y yields the Grandi's series, i.e.

$$S = x + y = \sum_{n=1}^{\infty} j^2 + \sum_{n=1}^{\infty} i^2 = (1 + 1 + 1 + \dots) + (-1 - 1 - 1 + \dots) = 1 - 1 + 1 - 1 + 1 - 1 + \dots = \sum_{n=0}^{\infty} (-1)^n$$

We can write out this series in two ways, i.e.

$$S = (1 - 1) + (1 - 1) + (1 - 1) + \dots + (1 - 1) = 0$$

and

$$S = (1 - 1) + (1 - 1) + (1 - 1) + \dots + (1 - 1) + 1 = 1$$

Thus, it appears that this sum has two 'values', namely, 0 and 1. However, if we also consider the geometric series

$$G = 1 + r + r^2 + r^3 + \dots = 1 + r(1 + r + r^2 + \dots) = 1 + rG \Rightarrow G = \frac{1}{1-r}, |r| < 1$$

then as $r \rightarrow -1$, $G \rightarrow \frac{1}{2}$. Under this limit, we can then write

$$S = \begin{cases} 1, & \text{or} \\ \frac{1}{2}, & \text{or} \\ 0. \end{cases}$$

where

$$\frac{1}{2} \equiv \lim_{\epsilon \rightarrow 0} \frac{1}{2 + \epsilon} = 0.49999999.... \quad (12)$$

thereby conforming to the condition required for the geometric series given above to converge, i.e. $|r| < 1$.

The Grandi's series can also be written as

$$S = y + x = \sum_{n=1}^{\infty} i^2 + \sum_{n=1}^{\infty} j^2 = (-1 - 1 - 1 - ...) + (1 + 1 + 1 + ...) = -1 + 1 - 1 + 1 - 1 + ...$$

In this case, we have

$$S = (-1 + 1) + (-1 + 1) + (-1 + 1) + \dots + (-1 + 1) = 0$$

and

$$S = (-1 + 1) + (-1 - +1) + (-1 + 1) + \dots + (-1 + 1) - 1 = -1$$

Further, we can consider the geometric series

$$G = -1 - r - r^2 - r^3 - \dots = -1 - r(1 + r + r^2 + \dots) = -1 - r(-G) = -1 + rG \Rightarrow G = \frac{-1}{1 - r}, |r| < 1$$

In this case, if we let $r \rightarrow -1$, then $G \rightarrow -\frac{1}{2}$ so that under this limit, we can write

$$S = \begin{cases} -1, & \text{or} \\ -\frac{1}{2}, & \text{or} \\ 0. \end{cases}$$

where the value of $\frac{1}{2}$ again conforms to Equation (12). Combining the results for the sum S , it is apparent that

$$S = \begin{cases} \pm 1, & \text{or} \\ \pm \frac{1}{2}, & \text{or} \\ \pm 0. \end{cases}$$

The Grandi series S has no sum in the conventional sense of convergence to a single specific value. Instead, it appears to have six values (if we include the trivial result that $0 = \pm 0$). Thus, we have the following three equations:

$$x + y = \pm 0 \quad (13)$$

$$x + y = \pm \frac{1}{2} \quad (14)$$

$$x + y = \pm 1 \quad (15)$$

Equations (13) and (15) are compatible with the Equation (14) given that if we add Equations (13) and (15) together, then we obtain Equation (14). Thus the equations are self-consistent.

Given Equation (11), Equation (13) is easily satisfied. However, we also have to satisfy Equations (14) and (15). In the former case, and, with regard to Equation (11), we have two choices. Either $x = -\frac{1}{2}$ and $y = \pm 0$ or $x = \pm 0$ and $y = \frac{1}{2}$. To satisfy Equation (15) in regard to Equation (11) requires that $y = \frac{1}{2}$ and $x = \frac{1}{2}$ or $x = -\frac{1}{2}$ and $y = -\frac{1}{2}$. This yields the following results:

$$\sum_{n=1}^{\infty} i^2 = \pm \frac{1}{2} \Rightarrow i^2 = \pm 1$$

and

$$\sum_{n=1}^{\infty} j^2 = \pm \frac{1}{2} \Rightarrow j^2 = \pm 1$$

given Equation (11).

These result appear to imply that $i^2 = \pm 1$. However, it should be appreciated that this paradox is a result of combining a non-standard result compounded in Equation (11) with the Grandi's series. Equation (11) has been derived from the Riemann zeta function and relies on the meromorphic properties of this function to consider what is in effect a divergent series. It is an example of a Ramanujan summation for assigning a value to a divergent series and is not an infinite sum in the conventional sense.

The Grandi's series is neither a convergent or a divergent summation but an indeterminate series. Thus, the above analysis relies on combining two non-standard results and the paradox must be understood within the context of these results. On the other hand, it should be noted that both the Grandi's series and the series for $\zeta(0)$ are examples of Ramanujan sums [18] when we can write

$$\sum_{n=1}^{\infty} 1^n \stackrel{\mathfrak{R}}{=} -\frac{1}{2} \quad \text{and} \quad \sum_{n=0}^{\infty} (-1)^n \stackrel{\mathfrak{R}}{=} \frac{1}{2}$$

where \mathfrak{R} denotes a Ramanujan sum. Thus, as a Ramanujan sum, Equation (11) is valid.

In the context of the paradox presented in this section, we now consider its effect on the study of a hypothetical concept in physics, namely, imaginary mass.

8 Tachyonic Fields

A Tachyonic field is one that is generated by particles with an imaginary mass [9]. The existence of such fields is currently only of hypothetical interest and there is continued debate as to whether imaginary mass particles can actually exist. One of the reasons for this is that imaginary mass particles can travel at faster than light speeds, therefore violating one of the underlying principles of physics, i.e. causality, in the sense that light speed is a universal upper bound [19], [20]. In this section, we consider the consequences of considering an imaginary mass im but whose square is $+m^2$ and not $-m^2$. The reason for this is that it forces a particle with an imaginary mass to conform with the principal of causality. To explain why this is the case, we revisit the relativistic energy equation as given in the following section.

8.1 The Relativistic Energy Equation

The relativistic energy equation (the energy-momentum relation) is a consequence of the special theory of relativity and expresses the square energy of a particle with a mass m as (e.g. [21] and [22])

$$E^2 = p^2 c^2 + m^2 c^4$$

where E , $p = mv$ and $c \simeq 2.99792458... \times 10^8 \text{ m} \cdot \text{s}^{-1}$ denote energy, momentum (for a particle with velocity v) and light speed, respectively. It is useful (in the sense of reducing 'equation clutter' due to the repetition of having to include physical constants) to use 'natural units' and set light speed to 1. This allows the energy equation to be expressed in the form (with $c = 1$)

$$E^2 = p^2 + m^2 \tag{16}$$

The causality principle is then associated with the universal upper bound on the velocity of a particle being 1. Thus, in the analysis that follows, $p := pc$ and $m := mc^2$. In this form, i.e. Equation (16), it is clear that E , p and m are quantities associated with a right-angle triangle, thereby confirming to Pythagoras' Theorem, a Theorem that is further quantified and justified by the relatively recent proof of Fermat's Last Theorem [23]. Thus, for positive energy,

$$E = \sqrt{p^2 + m^2}$$

Note that this equation can be written, using a binomial expansion, as

$$E = m \left(1 + \frac{p^2}{m^2} \right)^{\frac{1}{2}} = m \left(1 + \frac{p^2}{m^2} + \dots \right) = m + \frac{p^2}{2m} + \dots \simeq m + \frac{p^2}{2m}$$

which expresses the energy in terms of the sum of rest mass energy m and the non-relativistic or Newtonian energy $p^2/2m$. This result is applicable for any particle with a mass m but with a low velocity v such that $p^2/m^2 \ll 1$, i.e. $v^2 \ll 1$. The kinetic energy E_k is then defined as

$$E_k = E - m = \frac{p^2}{2m} \quad (17)$$

Imaginary Mass and Complex Energy The concept of an imaginary mass evolves if we consider Equation (16) to be a manifestation of the square amplitude in the complex plane with real axis p and imaginary axis im . If we consider the energy to be a complex value given by $E = p \pm im$, then Equation (16) is recovered if we take the square modulus of the complex energy, given that

$$E^2 \equiv |E|^2 = (p \pm im)(p \pm im)^* = (p \pm im)(p \mp im) = p^2 + m^2 \quad (18)$$

In this sense, an imaginary mass, by default implies a complex energy, both concepts being hypothetical within the ‘accepted standards’ of the physical world. Moreover, introducing an imaginary mass in this way has implications in regard to causality as shall now be shown.

Imaginary Mass and Causality Consider the energy E to be the rest mass energy of a particle with real mass M when $E = M$. Then, since the momentum of such a particle is $p = Mv$ where v is the velocity of a particle, we can write

$$\frac{1}{M} = \frac{v}{p} = \frac{1}{\sqrt{p^2 + m^2}}$$

so that

$$v = \frac{p}{\sqrt{p^2 + m^2}} = \frac{1}{\sqrt{1 + \frac{m^2}{p^2}}}$$

If $m = 0$, then $v = 1$ (light speed). For any other value $m > 0$, $v < 1$ (less than light speed). However, if $m := \pm im$, then

$$v = \frac{1}{\sqrt{1 - \frac{m^2}{p^2}}} \quad (19)$$

and now for any $m > 0$ where $m^2/p^2 < 1$, the velocity of the particle becomes greater than light speed. This is of course a bizarre result that does not conform to the central principle of the theory of relativity. So how can we make sense of this result?

Non-standard Imaginary Mass One approach to make sense of an imaginary mass is to assume that there are particles with an imaginary mass and that they can propagate at velocities greater than light speed. Another approach, which is the one considered in this work, is to assume that imaginary mass particles can exist but that they conform to the non-standard rule:

$$(\pm im)^2 = +m^2 \Rightarrow i^2 = +1 \quad (20)$$

This result does not of course conform to what is arguably the single most fundamental rule of complex analysis, a rule that is designed specifically to make the square of $\sqrt{-1}$ conform to a real number system inclusive of negative numbers from which $\sqrt{-1}$ arises naturally. However, introducing the rule that $i^2 = +1$ for a non-standard imaginary mass, ensures that an imaginary mass particle conforms to the inequality $v < 1$ in Equation (19) and is therefore causality preserving.

It is this break with a standard definition that is explored in the rest of this paper where we consider an imaginary mass to be the only physical entity that adheres to the non-standard result quantified in Equation (20). This result is taken to be a physical manifestation of the paradox considered in Section

7. Thus, in the material that follows, we consider the ramifications associated with a Tachyonic field generated by a particle with an imaginary mass subject to Equation (20). The key associated with the approach that is now taken, is to note that Equation (20) yields an incompatibility in regard to Equation (18) which becomes

$$E^2 \equiv |E|^2 = (p \pm im)(p \pm im)^* = (p \pm im)(p \mp im) = p^2 - m^2$$

and is not the relativistic energy equation (or Pythagoras' theorem). However, we note that

$$E^2 = (p \pm im)(p \pm im) = p^2 + m^2 \pm 2imp \quad (21)$$

does yield compatibility with Equation (16), if and only if we consider that the square energy is now a complex entity whose real component is $p^2 + m^2$, subject to an imaginary mass conforming to Equation (20). This idea has ramifications for the equations of relativistic quantum mechanics which is explored in the following sections.

9 Principal Equations of Quantum Mechanics

We now consider the principal partial differential equations that are fundamental to relativistic quantum mechanics. Such equations are essentially based on Equation (16) subject to the energy and momentum operators of quantum mechanics, namely, that [24]

$$\hat{E} \equiv i\hbar \frac{\partial}{\partial t} \text{ and } \hat{p} \equiv -i\hbar \nabla$$

respectively, where t denotes time, $\hbar = 1.054571817... \times 10^{-34}$ J · s is the Dirac constant, and, for unit vectors \hat{x} , \hat{y} and \hat{z} defining a three-dimensional Cartesian space,

$$\nabla = \hat{x} \frac{\partial}{\partial x} + \hat{y} \frac{\partial}{\partial y} + \hat{z} \frac{\partial}{\partial z}$$

For the sake of simplicity and clarity in regard to introducing the ideas that follow, we consider a one-dimensional model with natural units $\hbar = c = 1$. Further, we use the notation

$$\partial_x \equiv \frac{\partial}{\partial x}, \partial_t \equiv \frac{\partial}{\partial t}, d_x \equiv \frac{d}{dx} \text{ and } d_t \equiv \frac{d}{dt}$$

In the following sections, a brief review is given on some of the fundamental equations of relativistic quantum mechanics for the one-dimensional case. This material is presented to contextualise the field equations for the case when an imaginary mass is taken to conform with Equation (20) as discussed in Section 10.

9.1 The Klein-Gordon Equation

Using the energy and momentum operators of quantum mechanics, for a wave function $\Psi(x, t)$, Equation (16) is consistent (as a phenomenology) with the following wave equation

$$(\partial_x^2 - \partial_t^2 - m^2)\Psi(x, t) = 0 \quad (22)$$

Equation (22) is the Klein-Gordon equation (e.g. [25], [26] and [27]) and the wave function Ψ describes the Higgs field generated by a Higgs Boson [11]. The Higgs Boson is a particle that accounts for the mass m and is the only Scalar Boson that has been experimentally verified to date [13]. Note that for a quantum potential with potential energy denoted by V , Equation (16) extends to the form

$$(E - V)^2 = p^2 + m^2 \Rightarrow (-\partial_t^2 - 2iV\partial_t + V^2)\Psi = (-\partial_x^2 + m^2)\Psi$$

9.2 The Schrödinger Equation

The Schrödinger equation (e.g. [28] and [29]) is the non-relativistic equivalence of the Klein-Gordon equation and can be derived from the Klein-Gordon equation as follows. Let $\Psi(x, t) = \Phi(x, t) \exp(imt)$. Then

$$\begin{aligned}\partial_t \Psi &= \exp(imt)(im + \partial_t)\Phi, \\ \partial_t^2 \Psi &= \exp(imt)(\partial_t^2 + 2im\partial_t - m^2)\Phi\end{aligned}$$

and Equation (22) is given by

$$(\partial_x^2 - \partial_t^2 + 2im\partial_t)\Phi(x, t) = 0 \quad (23)$$

However, suppose that the kinetic energy defined by Equation (17) is small compared to the rest mass energy so that the effect of relativistic energies is negligible. Then, in the non-relativistic limit, $E_k \ll m$, or, using the energy operator of quantum mechanics,

$$|i\partial_t\Phi| \ll |m\Phi| \Rightarrow |\partial_t^2\Phi| \ll |im\partial_t\Phi|$$

In the context of this inequality, Equation (23) is reduced to

$$(\partial_x^2 + 2im\partial_t)\Phi(x, t) = 0 \quad (24)$$

which is Schrödinger's equation (for natural units when $\hbar = 1$) where the wave function Φ describes non-relativistic particles with Probability Density Function $|\Phi|^2$. This equation is of course the wave equation associated with the kinetic energy and momentum operators applied to Equation (17). For a potential V , the energy equation is

$$E_k - V = \frac{p^2}{2m} \Rightarrow i\partial_t\Phi = -\frac{1}{2m}\partial_x^2\Phi + V\Phi$$

9.3 The Fractional Shrödinger-Klein-Gordon Equation

Equations (22) and (24) both describe spin-less particles. In terms of the differential operators associated with these equations, Equation (24) is second order in space and first order in time whereas Equation (22) is second order in both space and time. Equation (24) describes non-relativistic quantum systems such as the electrons associated with atoms and molecules (subject to their interaction with a nuclear potential compounded in the potential energy V). Equations (22) describes Scalar Bosons such as Mesons which are hadronic subatomic particles composed of one quark and one antiquark, bound together by the strong interaction (subject to interaction with a nuclear potential). Thus, one may think of the difference between Equation (24) and Equation (22) as being the difference between atomic/molecular physics and nuclear physics, respectively.

In terms of the eigen-functions or standing wave patterns that Equations (24) and (22) describe (subject to an interaction with a potential), they can loosely be taken to represent the difference between the behaviour of an atom (a non-relativistic system) and the nucleus of an atom (a relativistic system) which provides the potential energy for the standing wave patterns associated with an electron cloud to evolve. In this sense, the distinct nature and associated characteristics of these equations are analogous to the distinct components associated with the basic Bohr model for an atom, i.e. a dense nucleus surrounded by an electron cloud.

Given Equations (24) and (22), it would appear that there are no intermediate component states (states that exist between the relativistic and non-relativistic regimes). So how can such states be modelled? The essential difference between Equations (24) and (22) relates to the time derivatives being first and second order, respectively. Thus, an approach to solving this problem is to consider the idea of introducing a fractional time derivative ∂_t^α where $1 < \alpha < 2$ to generate a Fractional Shrödinger-Klein-Gordon equation. On the basis of this approach, we can construct the equation [30]

$$\left[\left(\frac{1}{2m} \right)^{2-\alpha} \partial_x^2 + i^\alpha \partial_t^\alpha - (\alpha - 1)m^2 \right] \Psi(x, t) = 0$$

It is then clear that when $\alpha \rightarrow 1$ and $\alpha \rightarrow 2$, Equations (24) and (22) are recovered, respectively, for the common wave function Ψ .

9.4 The Dirac Equations

Given Equation (24), we can also consider the equation,

$$(\partial_x^2 - 2im\partial_t)\Phi^*(x, t) = 0$$

and hence write

$$\Phi^*(\partial_x^2 + 2im\partial_t)\Phi = 0 \text{ and } \Phi(\partial_x^2 - 2im\partial_t)\Phi^* = 0$$

Subtracting these two equations, we can write the result in the form

$$\partial_t\rho + \partial_xj = 0 \quad (25)$$

where

$$\rho = |\Phi|^2 \text{ and } j = \frac{1}{2im}(\Phi^*\partial_x\Phi - \Phi\partial_x\Phi^*)$$

Equation (25) is the one-dimensional continuity equation which relates the probability density ρ of the wave function Φ to the probability current density j . In this case, the probability density is positive definite and convective according to conservation law compounded in the continuity equation. Applying an equivalent analysis to Equation (22) does not result in the same conservation law. This is because the probability density function now becomes given by

$$\rho = \frac{1}{2im}(\Psi^*\partial_t\Psi - \Psi\partial_t\Psi^*)$$

which is not positive definite, meaning that the ρ can be both positive and negative and consequently incompatible with the concept of a probability density. It for this reason that a different approach to quantifying Equation (22) is required, one that allows a relativistic equation to be written in terms of E and not E^2 . This approach is the basis of the Dirac equations ([31] and [32]), as shall now be presented.

The basic idea is to consider an expression for the energy that is given by $E = Ap + Bm$, where A and B are arbitrary coefficients. Equation (16) is then given by

$$E^2 = A^2p^2 + B^2m^2 + ABmp + BAmp$$

In order for the square energy to be consistent with Equation (16), we require that $A^2 = B^2 = 1$ and $AB + BA = 0$. The only way to satisfy this requirement, is for A and B to become the (Pauli) matrices

$$A = \begin{pmatrix} 0 & 1 \\ 1 & 0 \end{pmatrix} \text{ and } B = \begin{pmatrix} 1 & 0 \\ 0 & -1 \end{pmatrix}$$

given that

$$A^2 = \begin{pmatrix} 0 & 1 \\ 1 & 0 \end{pmatrix} \begin{pmatrix} 0 & 1 \\ 1 & 0 \end{pmatrix} = \begin{pmatrix} 1 & 0 \\ 0 & 1 \end{pmatrix}, \quad B^2 = \begin{pmatrix} 1 & 0 \\ 0 & -1 \end{pmatrix} \begin{pmatrix} 1 & 0 \\ 0 & -1 \end{pmatrix} = \begin{pmatrix} 1 & 0 \\ 0 & 1 \end{pmatrix},$$

$$AB = \begin{pmatrix} 0 & 1 \\ 1 & 0 \end{pmatrix} \begin{pmatrix} 1 & 0 \\ 0 & -1 \end{pmatrix} = \begin{pmatrix} 0 & -1 \\ 1 & 0 \end{pmatrix} \text{ and } BA = \begin{pmatrix} 1 & 0 \\ 0 & -1 \end{pmatrix} \begin{pmatrix} 0 & 1 \\ 1 & 0 \end{pmatrix} = \begin{pmatrix} 0 & 1 \\ -1 & 0 \end{pmatrix}$$

In this case, the wave function ψ must take on not one but two states ψ_1 and ψ_2 so that with

$$\Psi = \begin{pmatrix} \psi_1 \\ \psi_2 \end{pmatrix} \text{ where } |\Psi|^2 = |\psi_1|^2 + |\psi_2|^2$$

we can write

$$i\partial_t\Psi = -iA\partial_x\Psi + mB\Psi$$

which represents two coupled equations for ψ_1 and ψ_2 given by

$$i\partial_t\psi_1 = -i\partial_x\psi_2 + m\psi_1 \text{ and } i\partial_t\psi_2 = -i\partial_x\psi_1 - m\psi_2$$

The function Ψ describes a ‘Spinor field’ where the two states ψ_1 and ψ_2 are taken to describe the ‘spin-up’ and ‘spin-down’ properties of an electron, an example of a ‘ $\frac{1}{2}$ -spin Fermion’. However, the concept of

a spin is merely a visual representation for a Spinor, in the same way that the Bohr model is a visual representation for an atom (in the non-relativistic case).

The key point about these Dirac equations is that in both cases, the probability density is a positive definite entity when defined in terms of the associated continuity equations that are given by

$$\partial_t \rho_1 = \psi_1 \partial_x \psi_2^* - \psi_1^* \partial_x \psi_2, \quad \rho = |\psi_1|^2$$

and

$$\partial_t \rho_2 = \psi_2 \partial_x \psi_1^* - \psi_2^* \partial_x \psi_1, \quad \rho = |\psi_2|^2$$

In other words, unlike the Klein-Gordon equation, the Dirac equations for ψ_1 and ψ_2 , conform to a conservation law determined by the continuity equation. However, there is another and seemingly equally valid approach that may be considered. This is addressed in the following section.

10 Formulation in the Complex Plane

Let $E = p \pm im$ where $i = \sqrt{-1}$. Any (complex) wave function ψ associated with this equation must also have two states as defined by $\pm i$. Let this two state wave function be denoted by

$$\Psi = \begin{pmatrix} \psi_{+i} \\ \psi_{-i} \end{pmatrix} \quad \text{where} \quad |\Psi|^2 = |\psi_{+i}|^2 + |\psi_{-i}|^2$$

Expressing the relativistic energy as a complex entity recovers Equation (16) if and only if we consider the square energy to be the square modulus of E since

$$EE^* = (p \pm im)(p \pm im)^* = (p \pm im)(p \mp im) = p^2 + m^2$$

This yields the field equations

$$\partial_t \psi_{+i} = -\partial_x \psi_{+i} + m\psi_{+i}$$

and

$$\partial_t \psi_{-i} = -\partial_x \psi_{-i} - m\psi_{-i}$$

which can be written as

$$\partial_t \begin{pmatrix} \psi_{+i} \\ \psi_{-i} \end{pmatrix} = -\partial_x \begin{pmatrix} \psi_{+i} \\ \psi_{-i} \end{pmatrix} + m \begin{pmatrix} 1 & 0 \\ 0 & -1 \end{pmatrix} \begin{pmatrix} \psi_{+i} \\ \psi_{-i} \end{pmatrix}$$

or as

$$(\partial_x + \partial_t - m\sigma)\Psi = 0$$

where

$$\sigma = \begin{pmatrix} 1 & 0 \\ 0 & -1 \end{pmatrix}$$

This approach provides a two-state wave function whose states are determined by $\pm im$. Further, the probability density is positive definite and given by

$$\rho = |\psi_{\pm i}|^2,$$

the continuity equation being given by

$$(\partial_t + \partial_x)\rho = \pm 2m\rho$$

An equally valid approach is to consider the complex energy equation $E = m \pm ip$ given that $|E|^2 = m^2 + p^2$ which yields the field equation

$$(\sigma \partial_x - i\partial_t - m\sigma)\Psi = 0$$

and the continuity equation

$$\partial_t \rho = \pm 2mj \quad \text{where} \quad j = \frac{1}{2im} (\Psi^* \partial_x \Psi - \Psi \partial_x \Psi^*)$$

The problem with either approach is that it introduces the concept of a complex energy through a particle having an imaginary mass and real momentum or an imaginary momentum and a real mass (i.e. a real mass with an imaginary velocity). These are concepts that are not required in the derivation of the Dirac equation. Moreover, as soon as we introduce the concept of an imaginary mass, causality is not preserved as compounded in Equation (19) for the case when m is replaced with $\pm im$.

One way to avoid this problem is to retain the Dirac equations and the approach to their construction. However, a complex plane formulation is an equally valid approach. In this case, the problem is avoided if we consider $E = m \pm ip$ instead of $E = p \pm im$. But then the latter case is also equally valid. So how can we make this equally valid complex energy equation generate field equations based on an assumed imaginary mass such that causality is preserved?

Suppose we attempt to generate self-consistency not through an equation for $|E|^2$ but for E^2 . In this case, for $E = p \pm im$

$$E^2 = p^2 - m^2 \pm 2imp$$

which is incompatible with Equation (16). However, if we let $(\pm im)^2 = +1$ rather than -1 we obtain

$$E^2 = p^2 + m^2 \pm 2imp \quad (26)$$

It is then clear that self-consistency with Equation (16) is achieved in terms of the real component of E^2 for this non-standard definition of the square of an imaginary mass. In this context, we now consider the modifications to the field equations presented in Section 9 that are required in order for Equation (26) to be satisfied.

10.1 Modified Klein-Gordon Equation

Using the energy and momentum operators $i\partial_t$ and $-i\partial_x$, respectively, the wave equation for $\Re[E^2] = p^2 + m^2$ yields Equation (22). However, for Equation (26), we obtain

$$(\partial_x^2 - \partial_t^2 - m^2 \pm 2m\partial_x)\Psi = 0 \quad (27)$$

As discussed earlier, the concept of particles with an imaginary mass leads to an incompatibility with the principle axiom of special relativity unless we describe them in terms of having an imaginary component im where $i^2 = +1$ which breaks with a fundamental convention. A consequence of this is that the Klein-Gordon equation evolves an extra term involving a spatial field gradient $\partial_x\Psi$. This equation is analogous to the Telegrapher's equation [33] which, for arbitrary real constants α and β is given by

$$(\partial_x^2 - \partial_t^2 - \alpha\partial_t - \beta^2)\Psi = 0$$

and is similar to the Klein-Gordon equation with dissipation in time [34]. However, in the case of Equation (27), the dissipation term is not in time but in space. Consequently, for the time independent case, the solution of

$$(d_x^2 - m^2 \pm 2md_x)\Psi(x) = 0$$

where $\psi(x) \rightarrow 0$ as $x \rightarrow 0$, and, for the initial condition $\psi(0) = 1$ is,

$$\psi(x) = \exp[-(\sqrt{2} - 1)mx], \quad x \geq 0$$

which is the solution to

$$(d_x^2 - m^2 - 2md_x)\psi(x) = 0, \quad \psi(0) = 1, \quad \psi(\infty) = 0$$

This solution is comparable to the time-independent solution to the (conventional) Klein-Gordon equation, i.e.

$$(d_x^2 - m^2)\psi(x) = 0, \quad \psi(0) = 1, \quad \psi(\infty) = 0$$

when

$$\Psi(x) = \exp(-mx), \quad x \geq 0$$

In the context of the analysis considered above, if imaginary mass particles are taken to exist then:

- (i) they travel faster than light speed which defies the fundamental physical principle of the theory of relativity;
- (ii) they conform to this fundamental physical principle but defy the law of imaginary numbers where $i^2 = -1$ is replaced with $i^2 = +1$ for an imaginary mass (and for mass alone).

In respect to the latter point above, the conventional Klein-Gordon equation adheres to $\Re[E^2] = p^2 + m^2$ where $\Im[E^2] = \pm 2mp$. As a consequence of this, the Klein-Gordon equation must be modified to include the effect of the imaginary component of the square energy. This has consequences for the characteristics of a Higgs Boson given that the Higgs field Ψ is now characterised not by $m^2\Psi$ but by $(m^2 + 2m\partial_x)\Psi$.

10.2 Modified Schrödinger Equation

By repeating the analysis given in Section 9.2 for Equation (27), the equivalent modified Schrödinger equation is given by

$$(\partial_x^2 + 2im\partial_t \pm 2m\partial_x)\Phi(x, t) = 0 \quad (28)$$

In this case, the Schrödinger equation includes an additional term which depends on the gradient of the wave function.

10.3 Non-standard Imaginary Mass and Euclidean Geometry

In regard to the (complex) energy equation $E = p \pm im$ where

$$E^2 = p^2 + m^2 \pm 2imp,$$

consider the case when we can write $E^2 = E - c$ for some complex value c which implies that

$$E = \frac{1 \pm \sqrt{1 - 4c^2}}{2}$$

We can then consider the complex plane iteration

$$p_{n+1} \pm im_{n+1} = p_n^2 + m_n^2 \pm 2im_np_n + c, \quad p_0 = m_0 = 0$$

For the case of $+i$, this iteration for the momentum and mass then conforms to the generation of the Euclid given in Figure 5. The region of non-divergence associated with this iteration for a complex energy $E = p + im$ where $(im)^2 = +m^2$ and variable c can then be said to be compatible with the generation of a Euclid in the sense of the iteration leading to the construction of a square. This leads to the fascinating idea that Euclidean geometry might be a manifestation of an imaginary mass which conforms to Equation (20). In other words, Euclidean geometry is predicated on the existence of a non-standard imaginary Higgs field.

11 Green's Functions

Green's function provide an intrinsic property of any and all wave field equations (i.e. a partial differential equations for a wave function) as they describe the free propagation of the wave field from one point in space-time to another. In this sense, the Green's function is a fundamental characteristic of a quantum field. Thus, in this section we consider the Green's function for Equation (22), which is a standard and well known result, and Equation (27), which is a non-standard result.

For a linear operator \mathcal{L} defining a one-dimensional partial differential equation

$$\mathcal{L}\Psi(x, t) = 0$$

the Green's function G is given by solving the equation [35]

$$\mathcal{L}G(x, t) = -\delta(x)\delta(t)$$

where δ is the one-dimensional Dirac delta function.

11.1 Time Independent Green's Functions

We consider the computation of the Green's function based on the Fourier transformation from time to frequency space when

$$G(x, t) = \frac{1}{2\pi} \int_{-\infty}^{\infty} g(x, \omega) \exp(i\omega t) d\omega \quad \text{and} \quad \delta(t) = \frac{1}{2\pi} \int_{-\infty}^{\infty} \exp(i\omega t) d\omega$$

where we use the non-unitary definition of a Fourier transform for the angular frequency ω .

For Equation (22), the Green's function required is given by the solution of

$$(\partial_x^2 + \omega^2 - m^2)g(x, \omega) = -\delta(x) \quad (29)$$

and for Equation (27) is given by

$$(\partial_x^2 + \omega^2 - 2m\partial_x - m^2)g(x, \omega) = -\delta(x) \quad (30)$$

where we consider the term $-2m\partial_x$ so that the solution conforms to the condition that $g(\pm\infty, \omega) = 0$. To solve either of these equations, we resort again to use of the Fourier transform and let

$$g(x, t) = \frac{1}{2\pi} \int_{-\infty}^{\infty} \tilde{g}(x, \omega) \exp(ikx) dk \quad \text{and} \quad \delta(x) = \frac{1}{2\pi} \int_{-\infty}^{\infty} \exp(ikx) dk$$

Equation (29) is then transformed to (expressed in terms of the Green's function \tilde{g})

$$\tilde{g}(k, \omega) = \frac{1}{k^2 - \omega^2 + m^2} \Rightarrow g(x, \omega) = \int_{-\infty}^{\infty} \frac{\exp(ikx) dk}{k^2 - \omega^2 + m^2} \quad (31)$$

Similarly, Equation (30) transforms to

$$\tilde{g}(k, \omega) = \frac{1}{k^2 - \omega^2 - 2imk + m^2} \Rightarrow g(x, \omega) = \int_{-\infty}^{\infty} \frac{\exp(ikx) dk}{k^2 - \omega^2 - 2imk + m^2} \quad (32)$$

Let us consider the integrals in Equations (31) and (32) for the case when $m = 0$. In this case the Green's function is well known and given by [35]

$$g(x, \omega) = \frac{i}{2\omega} \exp(i\omega x) \quad (33)$$

This is an expression for the 'free space' Green's function, i.e. the Green's function that is not subject to any boundary conditions. Further, this Green's function represents an out-going wave travelling away from the origin and is therefore referred to as the 'out-going Green's function', the in-going free space Green's function being given by

$$g(x, \omega) = -\frac{i}{2\omega} \exp(-i\omega x)$$

The Green's function describing both out-going and in-going waves is therefore given by

$$f(x, \omega) = \frac{i}{2\omega} \exp(i\omega x) - \frac{i}{2\omega} \exp(-i\omega x) = -\frac{\sin(\omega x)}{\omega}$$

The standard method of computing this function is through the application of contour integration to the integrals given in Equations (31) and (32) for $m = 0$. However, there is another approach that can be considered and is useful in regard to evaluating the integrals given by Equations (31) and (32) for $m \neq 0$. This approach involves the evaluation of the corresponding indefinite integral and the application of an

integral calculator. Using, for example, the online integral calculator available at [36], for example, we obtain

$$\int \frac{\exp(ikx)dk}{k^2 - \omega^2} = \frac{e^{i\omega x} \operatorname{Ei}[ix(k - \omega)] - e^{-i\omega x} \operatorname{Ei}[ix(k + \omega)]}{2\omega}$$

where $\operatorname{Ei}(x)$ is the Exponential Integral given by

$$\operatorname{Ei}(x) = \int_{-\infty}^x \frac{\exp(y)}{y} dy$$

It is then clear, by induction, that we can consider the function $i \exp(i\omega x)/2\omega$ based on this result, given knowledge of the known result obtained from contour integration of the corresponding improper integral, i.e. the integral for $k \in (-\infty, \infty)$. This is the approach that is taken in regard to the integrals given by Equations (31) and (32). Thus, using [36], we obtain (ignoring the constant of integration)

$$\begin{aligned} \int \frac{\exp(ikx)dk}{k^2 - \omega^2 + m^2} &= -\frac{e^{-i\sqrt{\omega^2 - m^2}x} [\operatorname{Ei}(ix(k + \sqrt{\omega^2 - m^2})) - e^{2i\sqrt{\omega^2 - m^2}x} \operatorname{Ei}(ix(k - \sqrt{\omega^2 - m^2}))]}{2\sqrt{\omega^2 - m^2}} \\ &\Rightarrow g(x, \omega) = i \frac{\exp(i\sqrt{\omega^2 - m^2}x)}{2\sqrt{\omega^2 - m^2}} \end{aligned} \quad (34)$$

Similarly, using [36] again, we obtain (ignoring the constant of integration)

$$\begin{aligned} &\int \frac{\exp(ikx)dk}{k^2 - \omega^2 - 2imk + m^2} = \\ &- \frac{e^{-(i\sqrt{\omega^2 - 2m^2} + m)x} [\operatorname{Ei}[x(i(k + \sqrt{\omega^2 - 2m^2}) + m)] - e^{2i\sqrt{\omega^2 - 2m^2}x} \operatorname{Ei}[x(i(k - \sqrt{\omega^2 - 2m^2}) + m)]]}{2\sqrt{\omega^2 - 2m^2}} \\ &\Rightarrow g(x, \omega) = i \frac{\exp(i\sqrt{\omega^2 - 2m^2}x)}{2\sqrt{\omega^2 - 2m^2}} \exp(-mx) \end{aligned} \quad (35)$$

In both cases, it is clear that for massless ‘particles’ the Green’s functions given by Equations (34) and (35) reduce to the form given by Equation (33). Further, both Green’s functions have the same functional form in regard to the variable ω other than the change from $\sqrt{\omega^2 - m^2}$ to $\sqrt{\omega^2 - 2m^2}$. However, in the case of Equation (35) the Green’s function is characterised by a negative exponential.

Reverting back from the natural units that have been used for this analysis and re-introducing the numerical values for the physical constants \hbar and c provided earlier, this negative exponential term becomes

$$\exp\left(-\frac{mc^2x}{\hbar}\right) = \exp(-amx) \text{ where } a \simeq 2.8427 \times 10^{42}$$

Thus, for an electron, say, with a mass $m = 9.1093837015(28) \times 10^{-31}$ kg, the length ℓ over which the Green’s function decays in amplitude by a factor of $\exp(-1)$ is given by $\ell \simeq 3.8616 \times 10^{-13}$ m, i.e. the order of 0.4 pico metres. This is significantly less than the diameter of a hydrogen atom by some three orders of magnitude and two orders of magnitude greater than the diameter of a hydrogen nucleus (the diameter of a hydrogen atom is approximately 1.06×10^{-10} m and the diameter of the nucleus is approximately 2.40×10^{-15} m). Thus, the propagation a scalar Boson associated with an imaginary mass subject to Equation (20) takes place over sub-atomic scales at least for the case when $\omega > \sqrt{2}mc^2$. This result is similar for the Green’s function associated with Equation (28) given that, using an identical approach to the one already discussed, we can show that

$$g(x, \omega) = i \frac{\exp[i\sqrt{m(2\omega - m)}x]}{2\sqrt{m(2\omega - m)}} \exp(-mx)$$

which is characterised by the same negative exponentiation when $\omega > mc^2/2$. Thus, both the relativistic and non-relativistic models for a wave function describing a particle with an imaginary mass subject to Equation (20), yield the same exponential decay characteristics in regard to the propagation of a particle through a one-dimensional free space.

11.2 Time-Dependent Green's Functions

For completeness, we now consider the time-dependent Green's function. These are obtained by Fourier inverting with regard to ω . For Equation (33), we are required to compute the integral

$$G(x, t) = \frac{1}{2\pi} \int_{-\infty}^{\infty} \frac{i}{2\omega} \exp(i\omega x) \exp(i\omega t) dt$$

We then note that [37]

$$\text{sgn}(t) \leftrightarrow \frac{2}{i\omega}$$

where \leftrightarrow denotes the transformation to the Fourier domain and

$$\text{sgn}(t) = \begin{cases} -1, & t < 0; \\ +1, & t > 0. \end{cases}$$

It is then clear that

$$\frac{i}{2\omega} \leftrightarrow -\frac{1}{4} \text{sgn}(t)$$

and hence

$$G(x, t) = -\frac{1}{4} \text{sgn}(x + t)$$

In the case of Equation (34), the time dependent Green's function is given by [38]

$$G(x, t) = \frac{1}{4\pi} [(1 - \sin(mt))(\delta(x + t) + \delta(x - t)) + mH(t - |x|)J_0(mu)], u = \sqrt{t^2 - x^2}$$

where $H(x) = [1 + \text{sgn}(x)]/2$ is the Heaviside step function and J_0 is the zero order Bessel function. Thus, in the case of Equation (35), by induction, the time dependent Green's function is given by

$$G(x, t) = \frac{1}{4\pi} [(1 - \sin(\sqrt{2}mt))(\delta(x + t) + \delta(x - t)) + \sqrt{2}mH(t - |x|)J_0(\sqrt{2}mu)] \exp(-mx)$$

12 Conclusions

The concept of an imaginary mass in physics is not new and is the basis for the hypothesis of a Tachyonic field. However, as soon as this idea is considered, causality fails. In order to prevent this, in this paper we have considered a break with the fundamental rule of complex analysis and let $i^2 = \pm 1$. This break with conformity in regard to the basic unit of imaginary numbers yields some interesting properties. These have been studied in the Section 6 and reveal that in the case of the non-standard Mandelbrot set, a square is formed with no self-affine boundary structures. Thus, in the context of the Mandelbrot set, the difference between letting $i^2 = +1$ and $i^2 = -1$ appears to be compounded in the difference between Euclidean and Fractal geometry, respectively, where, in both cases, the Hausdorff dimension is the same and given by 2.

By considering the effect of letting $i^2 = +1$ for an imaginary mass only, the properties of a Higgs field change, such that the principle of causality is maintained subject to both the relativistic energy and its square being complex entities. In this case, the wave function for the relativistic case has a two state solution but the Klein-Gordon equation requires modification which introduces an extra term involving the field gradient. The connectivity between this result and Euclidean geometry associated with the properties of iteration in the complex plane has very briefly been identified and flagged in Section 10.3. On a physical but purely phenomenological basis, this connectivity implies that Euclidean geometry might be a by-product of a universe consisting of imaginary mass particles that are causal entities for which Equation (20) is applicable. In this context, the paradox presented in Section 7 provides a possible mathematical basis for this form of non-standard analysis and the possible physical consequences thereof.

13 Further Analysis

The analysis considered in this paper is constrained by the one-dimension models that have been considered. Thus, an obvious extension to this work, is to develop models for the field equations in a two- and three-dimensional space. In such a development, the quaternion formulation of the Dirac equations [39] may be of value but based on representing the complex energy in the form (for fundamental quaternion units \mathbf{i} , \mathbf{j} and \mathbf{k})

$$E = im + \mathbf{i}p_x + \mathbf{j}p_y + \mathbf{k}p_z$$

where $p_x = -i\partial_x$, $p_y = -i\partial_y$ and $p_z = -i\partial_z$ define the three components of the field gradients in a three-dimensional Cartesian space. In this case, the scalar component of the quaternion is an imaginary mass which is once again required to conform to Equation (20) for the Euclidean norm to be positive definite in the sense that

$$\|E\|_2^2 = m^2 + p_x^2 + p_y^2 + p_z^2$$

Appendices

The functions given in this Appendix are provided to give the reader a guide to the basic programming used to implement the computational procedures discussed in this paper for computing the non-standard Mandelbrot and Julia sets. They are provided for interested readers to repeat the results presented, investigate the transient behaviour for different maps and to extend the computational methods discussed. Where possible, the notation used for array variables and constants are based on the mathematical notation used in this paper as are the acronyms used for the function names. The functions have not been exhaustively tested and do not include data I/O or processing error checks. Both the code and commentary have been somewhat condensed in order to comply with the format of this publication while minimising the number of pages required to present it. The software was developed and implemented using (64-bit) MATLAB R2020b with double precision floating point arithmetic.

Appendix A

The function that follows is a MATLAB function for computing and visualising the transient characteristics of the non-standard Mandelbrot set based on Equation (9).

```
function NSMS(meshsize,iterations,negxval,posxval,negyval, posyval,alpha)
%FUNCTION Non-Standard Mandelbrot Set (NSMS)
%
%INPUTS:
%meshsize - Size of (square) mesh used to compute the set.
%iterations - Number of iteration used to compute the set.
%negxval - lower negative bound on the real x-axis.
%posxval - upper positive bound on the real x-axis.
%negyval - lower negative bound on the imaginary y-axis.
%posyval - upper positive bound on the imaginary y-axis.
%alpha - a value between 1 and 2 inclusively where,
%alpha = 1 gives the standard Mandelbrot set with i^2=-1,
%alpha = 2 gives the non-standard Mandelbrot set with i^2=+1
%and 1<alpha<2 gives a transitory characteristic set.
%
%OUTPUT: Graphical presentation of the map using the 'jet' colour map
%
%EXAMPLE to generate a conventional Mandelbrot set on a square mesh of size
%1000 x 1000 for 100 iterations and a numerical range in the complex plane
%of [-2,2] x [-2,2]: Run NSMS(1000,100,-2,2,-2,2,1)
%
```

```
%Set complex plane meshgrid size.
[x,y] = meshgrid(linspace(negxval, posxval, meshsize),...
    linspace(negyval, posyval, meshsize));
%Set c as a complex array of size x * iy
c = x + 1i * y;
%Initialize complex variables
z = zeros(size(c)); k = zeros(size(c));
%Compute alpha
alpha=cos(alpha*pi)+1i*sin(alpha*pi);
%Start iteration process
for n = 1:iterations
    %Apply quadratic map modified by value of alpha
    z=real(z).^2+alpha*imag(z).^2+2*1i*real(z).*imag(z)+c;
    %Compute iteration k for case when abs(z) > 2 & k=0
    k(abs(z) > 2 & k == 0) = iterations - n;
end
%Display image of set in Figure 1 using function 'imagesc'
figure(1), imagesc(k),
colormap jet %Use colour map 'jet'
set(gca,'XTick',[], 'YTick', [])%Turn off ticks for both axis.
pbaspect([1 1 1])%Use uniform aspect ratio for display
```

Appendix B

The .m code that follows is a MATLAB function for computing and visualising the transient characteristics of an arbitrary complex map $f(z)$ which must be constructed prior to running the function as an input to the function.

```
function NSFS(meshsize,iterations,negxval,posxval,negyval,posyval,map)
%FUNCTION Non-Standard Function Set (NSFS)
%
%INPUTS
%meshsize - Size of (square) mesh used to compute the set.
%iterations - Number of iteration used to compute the set.
%negxval - lower negative bound on the real x-axis.
%posxval - upper positive bound on the real x-axis.
%negyval - lower negative bound on the imaginary y-axis.
%posyval - upper positive bound on the imaginary y-axis.
%alpha - a value between 1 and 2 inclusively where,
%alpha = 1 gives the standard Mandelbrot set with  $i^2=-1$ ,
%alpha = 2 gives the non-standard Mandelbrot set with  $i^2=+1$ 
%and  $1<\alpha<2$  gives a transitory characteristic set.
%map - iteration function
%
%OUTPUT: Graphical presentation of the map using the 'jet' colour map
%
%EXAMPLE to generate the conventional Julia set for  $c=-0.4-i0.6$ 
%over a mesh of size 1000 x 1000 for 100 iteration and a numerical range
%in the complex plane of  $[-2,2] \times [-2,2]$ , set the corresponding function
% $f(z)$  as  $f = @(z) z.^2 - 0.4 - 1i*0.6$ ; and then run  $NSFS(1000,100,-2,2,-2,2,f)$ ;
%
%Set complex plane meshgrid size.
[x,y] = meshgrid(linspace(negxval, posxval, meshsize),...
    linspace(negyval, posyval, meshsize));
```

```
%Initialise complex array z.
z = x + 1i * y;
%Initialise complex variable
k = zeros(size(z));
%Start iteration process
for n = 1:iterations
    %Apply iteration to input map
    z=map(z);
    %Compute iteration k for case when abs(z) > 2 & k=0.
    k(abs(z) > 2 & k == 0) = iterations - n;
end
%Display image of set in Figure 1 using function 'imagesc'
figure(1), imagesc(k),
colormap jet %Use colour map 'jet'
set(gca,'XTick',[], 'YTick', [])%Turn off ticks for both axis.
pbaspect([1 1 1])%Use uniform aspect ratio for display
```

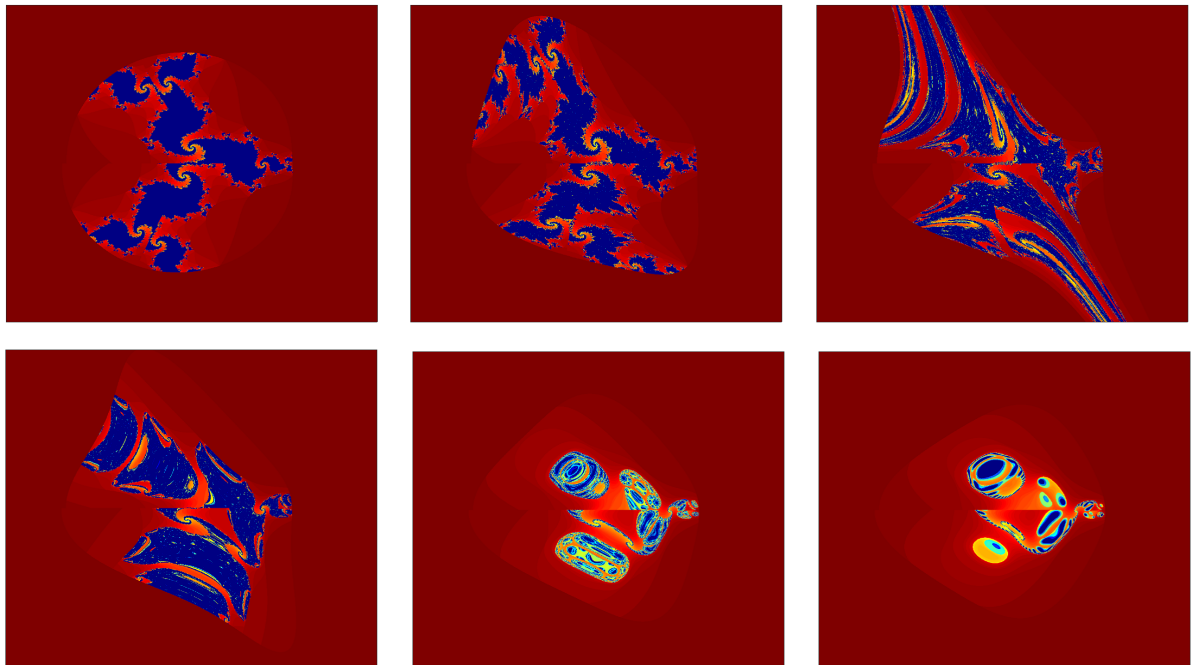


Figure 9. Transitions of the set based on the iteration given by Equation (36) for $\alpha = 1, 1.2, 1.4, 1.6, 1.8, 2$ (top-left through to lower-right, respectively). The set is computed for $c = 0.268 + 0.06i$, $x \in [-4, 2]$ and $iy \in [-3i, 3i]$ where x and iy are the horizontal and vertical axes in the complex plane, respectively. In this example, 100 iterations are performed using a mesh size of $10^3 \times 10^3$. The maps are colour coded using the MATLAB ‘jet’ colour map.

As an example of the utilisation of this function, consider the map

$$f : z \rightarrow f(z) = \frac{(z^2 + z)}{\log(z)} + c, \quad z \in \mathbb{C}$$

Using the approach considered in Section 6.3, the transient properties of this map are explored using the iteration

$$z_{n+1} = \frac{\Re[z]^2 + \exp(i\alpha\pi)\Im[z]^2 + 2i\Re[z]\Im[z] + z}{\log(z)} + c \quad (36)$$

where $\alpha \in [1, 2]$. This is undertaken by constructing the following .m code

```
alpha=value;
alpha=cos(alpha*pi)+1i*sin(alpha*pi);
f = @(z) ((real(z).^2+alpha*imag(z).^2+2*1i*real(z).*imag(z)+z)./log(z))+c;
```

where **value** is the numerical value of $\alpha \in [1, 2]$ and **c** is the complex constant. Figure 9 shows an example of the transitions associated with Equation (36) for $c = 0.268 + 0.06i$ and $\alpha = 1, 1.2, 1.4, 1.6, 1.8, 2$ with $x \in [-4, 2]$ and $iy \in [-3i, 3i]$.

Acknowledgements The author acknowledges the support of the Science Foundation Ireland; the School of Electrical and Electronic Engineering, Technological University Dublin; the School of Mathematics, Statistics and Computer Science, University of KwaZulu-Natal; the Department of Computer Science, Faculty of Natural Sciences, University of Western Cape and the Faculty of Arts, Science and Technology, Wrexham Glyndwr University of Wales.

References

1. I. Stewart and D. Tall, “Complex Analysis”, Edition 2, Cambridge University Press, 2018. ISBN: 978-1-43679-3
2. A. Douady and J. H. Hubbard, “Étude Dynamique des Polynômes cComplexes”, Société Mathématique de France, 2007. Available at: <http://pi.math.cornell.edu/~hubbard/OrsayFrench.pdf>
3. B. Mandelbrot, “The Fractal Geometry of Nature”, W. H. Freeman and Co., 1983. ISBN: 978-0-7167-1186-5
4. Euclid, “Elements”, (Eds. D. Densmore and T. L. Heath), Green Lion Press, 2002. ISBN: 978-1-888009-19-4
5. L. Carleson and T. W. Gamelin, “Complex Dynamics”, Springer 1993. ISBN: 978-0-387-97942-7
6. A. F. Beardon, “Iteration of Rational Functions”, Springer 1991. ISBN: 0-387-95151-2
7. H. M. Edwards, “Riemann’s Zeta Function”, Academic Press, 1974. ISBN-10: 0-486-41740-9 .
8. G. T. Bagni, “Infinite Series from History to Mathematics Education”, International Journal for Mathematics Teaching and Learning, 2005. Available at: <https://web.archive.org/web/20061229024056/http://www.cimt.plymouth.ac.uk/journal/bagni.pdf>
9. G. Feinberg, G. (1967). “Possibility of Faster-Than-Light Particles”. *Physical Review*, vol. 159, no. 5, pp. 1089?1105, 1967.
10. W. Greiner, “Relativistic Quantum Mechanics: Wave Equations” (Edition 3), Springer Verlag, 2000, ISBN: 3-5406-74578.
11. G. Bernardi, M. Carena and T. Junk, “Higgs bosons: Theory and searches”, Review: Hypothetical particles and Concepts. Particle Data Group, 2007. Available at: https://pdg.lbl.gov/2008/reviews/higgs_s055.pdf
12. P. W. Higgs, “Broken Symmetries and the Masses of Gauge Bosons”, Physical Review Letters, vol. 13 , no. 16, pp. 508?09, 1964.
13. G. Aad et al. “Combined Measurement of the Higgs Boson Mass in pp Collisions at $\sqrt{s}= 7$ and 8 TeV with the ATLAS and CMS Experiments”, Physical Review Letters, 114, 191803, 2015. Available at: <https://journals.aps.org/prl/abstract/10.1103/PhysRevLett.114.191803>
14. J. W. Milnor, “Dynamics in One Complex Variable”, Edition 3, *Annals of Mathematics Studies 160*, Princeton University Press 2006. Available at: <https://arxiv.org/abs/math/9201272>
15. E. Demidov, “The Mandelbrot and Julia sets Anatomy”, A virtual investigation with interactive pictures, 2003. Available at: <https://www.ibiblio.org/e-notes/MSet/Contents.htm>
16. M. Michelitsch and O. E. Rössler, “The ‘Burning Ship’ and Its Quasi-Julia Sets”. In: *Computers & Graphics*, vol. 16, no. 4, pp. 435-438, 1992.
17. MATLAB, Mathematical Computing Software, The MathWorks Inc., 2020. Available at: <https://uk.mathworks.com/products/matlab.html>.
18. B. C. Berndt, “Ramanujan’s Notebooks”, *Ramanujan’s Theory of Divergent Series*, Springer, 1985. Available at: <https://www.sussex.ac.uk/webteam/gateway/file.php?name=ramanujans-notebooks.pdf&site=454>
19. R. S. Vieira, “An Introduction to the Theory of Tachyons”, *Rev. Bras. Ens. Fis.* vol. 34, no. 3, pp. 1-17, 2011. Available at <https://arxiv.org/pdf/1112.4187.pdf>
20. J. M. Hill and B. J. Cox, “Einstein’s Special Relativity Beyond the Speed of Light”, *Proc. R. Soc. A* vol. 468 (2148), pp. 4174?4192, 2012. Available at: <https://royalsocietypublishing.org/doi/10.1098/rspa.2012.0340>
21. J. R. Forshaw and A. G. Smith, “Dynamics and Relativity” Wiley, 2009. ISBN 978-0-470-01460-8
22. D. McMahon, “Relativity. Demystified” McGraw-Hill, 2006. ISBN 0-07-145545-0

23. N Boston, "The Proof of Fermat's Last Theorem", University of Wisconsin, 2003. Available at: <https://www.math.wisc.edu/~boston/869.pdf>
24. N. Zettili, "Quantum Mechanics: Concepts and Applications", Edition 2, Wiley, 2009. ISBN: 978-0-470-02678-6
25. O. Klein, "Quantentheorie und fünfdimensionale Relativitätstheorie", *Zeitschrift für Physik*, vol. 37, no. 12, pp. 895-906, 1926. Available at: <https://edition-open-sources.org/media/sources/10/10/sources10chap8.pdf>
26. W. Gordon, "Der Comptoneffekt nach der Schrödingerschen Theorie", *Zeitschrift für Physik*, vol. 40, 117-133, 1926. Available from: <https://link.springer.com/article/10.1007%2FBF01390840>
27. S. Weinberg, "The Quantum Theory of Fields", Cambridge University Press, 2002. ISBN 0-521-55001-7
28. E. Schrödinger, "An Undulatory Theory of the Mechanics of Atoms and Molecules" *Physical Review*. vol. 28 no. 6, pp. 1049?1070, 2026. Available at: <https://web.archive.org/web/20081217040121/http://home.tiscali.nl/physis/HistoricPaper/Schroedinger/Schroedinger1926c.pdf>
29. E. Schrödinger, "Quantization as an eigenvalue problem," *Annalen der Physik*, vol. 489, no. 79, 1926.
30. J. M. Blackledge and B. Babajanov, "The Fractional Schrödinger-Klein-Gordon Equation and Intermediate Relativism", *Mathematica Eterna*, vol. 3, no. 8, 601-615, 2013. Available from: <https://www.longdom.org/articles/the-fractional-schrodingerkleingordon-equation-and-intermediate-relativism.pdf>
31. P. A. M. Dirac, "The quantum theory of the electron, Part 1," *Proc. R. Soc. (London) A*, vol. 117, pp. 610-612, 1928.
32. P. A. M. Dirac, "The quantum theory of the electron, Part II," *Proc. R. Soc. (London) A*, vol. 118, pp. 351-361, 1928.
33. Telegrapher's Equation, Wikipedia, 2020. Available at: https://en.wikipedia.org/wiki/Telegrapher%27s_equations
34. A. Giusti, "Dispersive Wave Solutions of the Klein-Gordon equation in Cosmology", *Scuola di Scienze Corso di Laurea in Fisica*, University of Bologna, 2013, Available at: <https://core.ac.uk/download/pdf/31155754.pdf>
35. G. Evans, J. M. Blackledge and P. Yardley, "Analytic Solutions to Partial Differential Equations", Springer, 1999. ISBN: 2540761241
36. Integral Calculator. Available: <https://www.integral-calculator.com/>
37. Fourier Transform, Wikipedia, 2020. Available at: https://en.wikipedia.org/wiki/Fourier_transform; Section 15: Tables of Important Fourier Transforms, Distributions; 15.4 One-Dimensional, Transformation 312.
38. Green's Function. Available: https://en.wikipedia.org/wiki/Green%27s_function
39. M. H. Silvis, "A Quaternion Formulation of the Dirac Equation", Centre for Theoretical Physics, University of Groningen, 2010. Available at: <https://mauritssilvis.nl/publications/silvis-rug10.pdf>